Iranian Journal of Chemistry and Chemical Engineering (IJCCE)

Enhancing Structural Surface Durability in Building Facades with Hyaluronic Acid Nanofiber Coatings

Lei Lei[1*], Shaolei Song[1], Yan Wang[1]

1, School of Civil Engineering, Xuzhou University of Technology, Xuzhou, Jiangsu, 221000, China

***Corresponding author's Email:** e_i27094@163.com

Abstract

Ensuring the long-term durability of building facades is crucial for maintaining their structural integrity and promoting sustainability. This study was aimed to explore the effectiveness of incorporating hyaluronic acid (HA) nanofiber reinforced coatings as a means of enhancing facade durability. The coatings were fabricated by adding HA nanofibers, ranging from 0-3 wt.%, to commercially available acrylic-silicone coating substrates. Standardized techniques were employed to assess the elastic modulus, compressive strength, and impact resistance of the resulting coatings. Additionally, an artificial neural network (ANN) was developed to predict these properties for new combinations of HA and facades. The inclusion of HA nanofibers had a significant concentration-dependent influence on the mechanical properties of the coatings. Increasing the HA loading led to proportional improvements in the elastic modulus, with enhancements of up to 22% observed at a 3 wt.% of HA loading. Likewise, the highest HA content resulted in an 18% increase in compressive strength. The impact toughness also exhibited a progressive rise, demonstrating a 29% higher energy absorption for the 3 wt.% HA compared to the unmodified control coating. The implemented ANN demonstrated its ability to accurately capture the dose-dependent patterns and effectively predict relevant properties of compositions that were not subjected to experimental evaluation. In conclusion, the proficient dispersion of HA nanofibers emerged as a crucial factor in fortifying the facades, establishing a harmonious interplay at the nanoscale level, ultimately augmenting their long-term resilience.

Keywords: *Hyaluronic acid nanofibers; Coating; Mechanical properties; Artificial neural network; Nanoreinforcement*

1- Introduction

The urban landscape and spaces are greatly influenced by buildings and their facades [1-3]. However, prolonged exposure to outdoor environmental factors such as weather conditions, pollutants, and moisture can cause deterioration of building facades over time, compromising both their structural integrity and aesthetic appeal. It is crucial to prioritize the maintenance of durable and resilient facades due to their significance in terms of structural safety, economic considerations, and sustainable architectural design [4]. Consequently, the exploration of advanced coating materials that can enhance the durability of facades has emerged as a vital area of research with substantial potential [5-9].

Previous research has focused on exploring diverse approaches to improve the long-lasting characteristics of exterior building facades [10-15]. To enhance mechanical performance, coating substrates have been reinforced with fiber materials like carbon, glass, and basalt [16-22]. Moreover, the incorporation of nanoparticles and nanofibers of ceramics, metals, and polymers within coating matrices has been investigated to augment their properties, such as strength and toughness [23-27]. Nevertheless, concerns persist regarding the potential toxicity and environmental impact associated with certain nanomaterial reinforcements.

Naturally occurring compounds have gained attention due to their inherent biodegradability and biocompatibility [28, 29].

Hyaluronic acid nanofibers are minuscule fibers composed of the glycosaminoglycan polymer known as hyaluronic acid [30-32]. Recent investigations were dedicated to the development of environmentally-friendly nanocoatings based on HA for the construction of resilient exteriors of buildings. Entekhabi et al. [33] employed electrospinning to fabricate composite coatings reinforced with HA nanofibers, examining the impact of HA content on mechanical properties. Fabrication of epoxy nanocomposites with varying loadings of HA nanoparticles and exploring their anti-corrosion performance, when even a mere 1 wt.% inclusion of HA led to enhanced corrosion resistance by reducing coating permeability and reinforcing barrier properties, is investigated in some studies [34].

To evaluate the dynamic mechanical behavior and water resistance of epoxy composites, Wu et al. [35] investigated the influence of HA fillers. The results showed that HA significantly augmented the storage modulus and glass transition temperature, while concurrently reducing the rate of water absorption due to the surface's increased hydrophilicity. In other study, HA nanoparticles embedded in a polyurethane acrylate matrix were evaluated, examining the effects of loadings ranging from 0 to 5 wt.% on mechanical, tribological and barrier properties [36]. The results indicated that HA nanoparticles contributed to enhanced elastic modulus, tensile strength and wear resistance. Furthermore, at a 3 wt.% HA loading, improved oxygen and water vapor barrier effects were observed.

Prior research has highlighted the benefits of incorporating HA nanoreinforcements to enhance coating properties; however, certain limitations remain unaddressed. Limited exploration has been conducted regarding the effects of varying HA contents, and previous studies have primarily utilized HA nanofibers as surface treatments or intermediate layers rather than directly incorporating them within exterior facade coating substrates. It is crucial to develop HA nanofiber composite coatings that are easy to apply and compatible with diverse facade designs to maximize their potential benefits.

To address these gaps, this study is aimed to systematically investigate the influence of varying weight percentages (ranging from 0.5 to 3%) of HA nanofibers incorporated directly in model exterior facade coating substrates. A comprehensive range of HA loadings was evaluated using standardized testing methods to assess their impact on coating properties. Furthermore, an ANN was developed and trained to predict mechanical attributes for new combinations of HA and facades, providing insights into optimizing HA nanofiber contents. Composite specimens were prepared by blending pre-processed HA nanofibers with acrylic-silicone matrices commonly used in architectural applications. Standardized characterization techniques were employed to evaluate the elastic modulus, compressive strength, and impact resistance of the coatings. The study is aimed to address key questions regarding the relations between HA dosage, mechanical response, and the effectiveness of the coatings in shielding against degradation.

The findings of this investigation hold significant potential for informing material designers and architects in the development of customized facade solutions that take into account various service conditions. By incorporating environmentally-sustainable HA nanomodification, this study contributes to the development of durable and resilient building envelopes, reducing future maintenance demands and enhancing long-term sustainability. Additionally, the results advance the fundamental understanding of nanoreinforcement mechanisms through quantitative analysis. Therefore, this study addresses existing limitations, offers practical benefits, and contributes to the theoretical understanding of HA nanofiber reinforced coatings in the context of exterior facades. Therefore, this study seeks to advance the field by systematically exploring a wider range of HA loadings directly incorporated within coating substrates commonly applied to building facades. Standardized quantitative techniques are employed to elucidate concentration-responsive trends and optimize HA content. Additionally, an artificial neural network model is developed that can predict material properties to inform improved material design.

2- Materials and Methods

2.1- Materials

The selected exterior facade coating substrates for this study consisted of commercially available acrylic-silicone formulations suitable for architectural applications. The choice of acrylic-silicone

materials was motivated by their desirable properties, including weather resistance, flexibility, adhesion, and UV stability [37-39]. The specific coating substrates used, namely Bilyfaçade XP2 and Bilyfaçade XP4, were obtained from Bily Coatings and represented two distinct composition variants.

Acrylic-silicone coatings like Bilyfaçade XP2 and Bilyfaçade XP4 are commonly employed in the construction industry due to their ability to balance performance attributes with reasonable cost. Bilyfaçade XP2 comprises 60% acrylic polymer, 30% silicone resin, and mineral fillers, providing good moisture resistance while exhibiting moderate thermal shock endurance. In contrast, Bilyfaçade XP4 incorporates organic pigments and rheology modifiers, replacing 20% of the mineral fillers. This modification is appropriate to enhance color retention and workability during application, albeit at the expense of some moisture permeability.

Regenerated medical grade sodium hyaluronate, obtained from Bloomage Biotechnology (China), was used as the source of hyaluronic acid for this study. HA is a linear polysaccharide composed of repeating disaccharide units of D-glucuronic acid and N-acetyl-D-glucosamine.

To fabricate the composites, the HA was first processed into nanofibers using the electrospinning technique. In brief, an 8% w/v HA solution was prepared by dissolving the powder in a mixture of formic acid and water at a 1:1 volume ratio. The solution was then loaded into a syringe pump, which operated at a flow rate of 1 mL/h. A voltage of 15 kV was applied between the needle tip and a rotating collector. After the solvent evaporation, nanofibers in the diameter range of 100-300 nm were successfully produced, as confirmed by scanning electron microscopy (SEM) imaging.

The estimated chemical composition ranges of the two specific facade coating substrates are provided in Table 1. This information is based on data provided by the manufacturer and supported by Fourier Transform Infrared Spectroscopy (FTIR) and thermal analysis studies conducted on similar acrylic-silicone systems. While minor formulation variations may exist between production batches, the primary components of the coating substrates are as outlined.

Table 1: Estimated chemical composition ranges of exterior facade coating substrates.

Coating Substrate	Acrylic Polymer (%)	Silicone Resin (%)	Mineral Fillers (%)	Organic Pigments (%)
Bilyfaçade XP2	55-65	25-35	5-10	-
Bilyfaçade XP4	45-55	20-30	5-10	5-10

2.2- Fabrication of HA nanofiber coatings

Prior to incorporating them into the exterior facade coating substrates, hyaluronic acid nanofibers were generated using the electrospinning technique. The experimental setup for this study consisted of a high voltage power supply, syringe pump, and rotating collector, as shown in Figure 1.

To prepare the HA solution, sodium hyaluronate powder was dissolved in a mixture of formic acid and deionized water at a 1:1 volume ratio, resulting in an 8% w/v concentration. Formic acid was selected as the electrospinning solvent due to its efficient ability to dissolve HA while remaining non-toxic and biodegradable. The solution was loaded into a 5 mL syringe equipped with a 21-gauge steel needle (the size of needle). The positive electrode of the high voltage supply was connected to the needle tip, while the rotating drum collector served as the ground electrode.

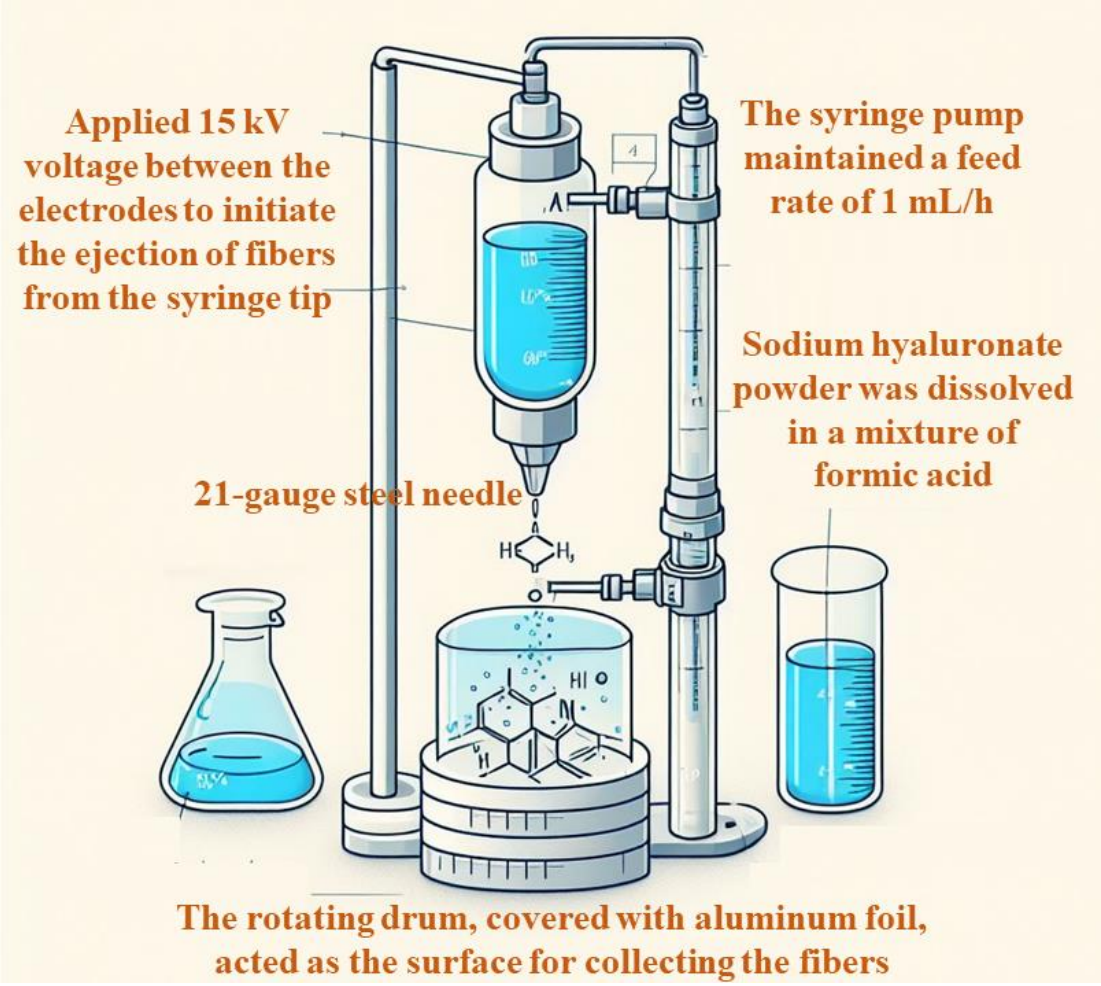

Figure 1: illustrates a schematic diagram of the electrospinning setup employed for the fabrication of HA nanofibers.

A voltage of 15 kV was applied between the electrodes to initiate the ejection of fibers from the syringe tip. The syringe pump maintained a feed rate of 1 mL/h. The rotating drum, covered with aluminum foil, acted as the surface for collecting the fibers. Through preliminary experiments, it was determined

that these spinning parameters resulted in uniform, bead-free HA nanofibers without issues of solvent dripping, fiber breaking, or jet instability. The electrospun mats were thoroughly dried in a fume hood to remove any residual solvent before further utilization.

The morphology and dimensions of the electrospun HA nanofibers were analyzed using scanning electron microscopy, as described in Section 3.1 of this study. Typically, the nanofibers exhibited average diameters ranging from 150 to 250 nm. The SEM images revealed smooth surfaces and the absence of structural defects, indicating the consistent and high-quality nature of the electrospinning process.

Subsequently, the HA nanofibers were incorporated into the exterior facade coating substrates to create composite panels. Different weight percentages of HA nanofibers, namely 0.5, 1, 2 and 3%, were added to the Bilyfaçade XP2 and XP4 coating substrates. Additionally, a control sample without any nanofiber addition was prepared for comparison. Prior to composite fabrication, the HA nanofiber mats, which had been pre-processed, were uniformly mixed with the respective Bilyfaçade XP2 and XP4 coating substrates.

To ensure even distribution of the nanofibers, the coating mixtures underwent thorough stirring. Each mixture was then cast into silicone molds measuring 30 cm x 30 cm x 2 mm to produce flat composite panels after the solvent had evaporated.

As previously mentioned, these panels were utilized for evaluating various properties using standardized testing protocols. In Figure 2 are the composite coating specimens reinforced with HA nanofibers, which were labeled according to the HA content and the composition of the facade substrate. These specimens served as test samples for investigating the impact of nanofiber loading levels on mechanical properties, including elastic modulus, compressive strength, and impact resistance, as detailed in Sections 2.4.1 and 2.4.2.

The fabrication method employed in this study facilitated the consistent preparation of composite coating specimens with controlled and uniform dispersion of HA nanofibers, allowing for systematic evaluation. Compared to blending micro- or macro-sized HA particles, the incorporation of nanoscale electrospun fibers provides enhanced reinforcement due to their high aspect ratio and surface area [40]. The straightforward casting technique used to add HA nanofibers also simulates their potential real-world application as environmentally friendly modifiers in exterior facade coating formulations.

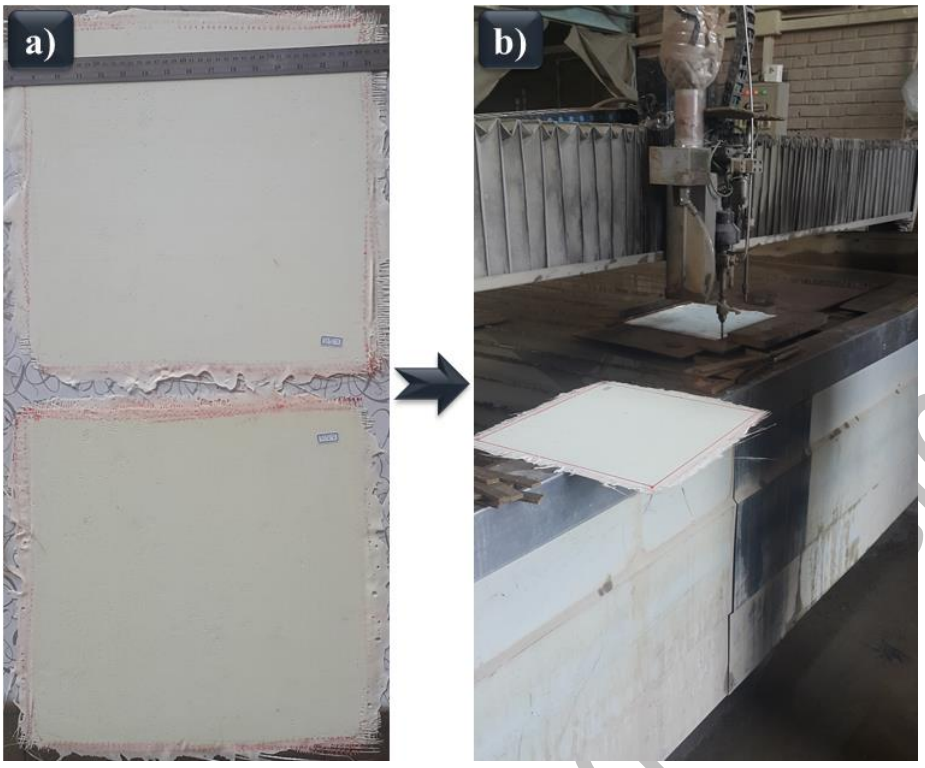

Figure 2: a) Composite coating specimens reinforced with HA nanofibers, labeled based on fiber content and substrate type, and b) cutting specimens based on test's standards for evaluating mechanical properties.

2.3- Morphological characterization

The field emission scanning electron microscopy (FESEM) technique was employed to analyze the morphology and dimensions of the electrospun HA nanofibers. To enhance conductivity, the fiber mats were coated with a thin layer of gold using a sputter coater prior to imaging. Imaging was conducted using a Zeiss Sigma 300 FESEM operating at 5 kV.

FESEM is a powerful tool for visualizing and examining nanoscale structures by utilizing an electron beam's interaction with samples [41-45]. It is essential to characterize fiber morphology and distribution using techniques like FESEM to assess the reproducibility of the electrospinning process and ensure fiber quality [46, 47]. In this study, FESEM provided detailed information about fiber morphology, diameter range, and the presence or absence of defects.

Digital images were captured at magnifications ranging from 10,000X to 50,000X, and they were subsequently analyzed using ImageJ software. The fiber diameters were measured at 10 randomly selected locations across each FESEM image to obtain statistically significant average diameter values. This analysis helped evaluate the uniformity of the fibers and the effectiveness of the electrospinning parameters employed for fabricating HA nanofibers.

2.4- Mechanical property testing

2.4.1- Elastic modulus and compressive strength

Mechanical properties of the composite coating specimens, including elastic modulus and compressive strength, were evaluated using standardized mechanical testing methods. The elastic modulus measurements were conducted following ASTM D638 guidelines, employing an Instron 5944 universal testing machine equipped with a 10 kN load cell from AixaccteFMC, Germany. The tests were performed under ambient conditions at a crosshead speed of 1 mm/min.

To ensure consistency, five dumbbell-shaped test samples were prepared from the flat composite panels using a waterjet machine, adhering to the dimensions specified in ASTM D638 Type V. Prior to testing, a 25 mm gauge length extensometer was affixed to the central portion of each specimen to accurately measure strain. The elastic modulus, which represents the material stiffness, was calculated by determining the slope of the initial linear region of the stress-strain curve within a strain range of 0.005-0.0025% [48, 49]. The setup for the tensile testing is presented In Figure 3, illustrating a specimen fixed in the Instron grips with an attached extensometer for strain measurement.

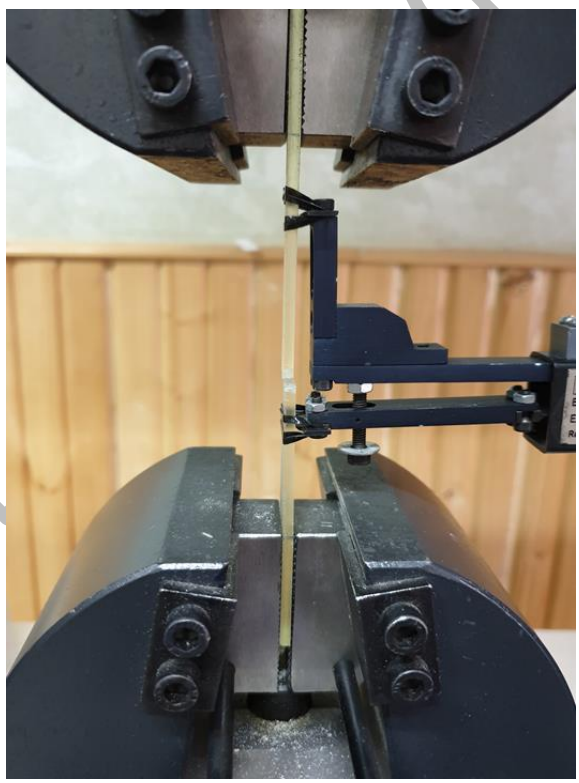

Figure 3: Tensile testing setup showing a specimen mounted in the tensile testing grips.

The determination of compressive strength followed the guidelines of ASTM D695, utilizing specimens with dimensions conforming to Type I configuration, which were cut from the composite panels. Tests were conducted using an Instron 4469 universal tester under the same environmental conditions at a speed of 1 mm/min.

For each composition, five cylindrical specimens were positioned and loaded along their longitudinal axis between steel platens in the testing machine until failure occurred. The maximum load sustained before failure was recorded and used to calculate the compressive strength. These values, along with the elastic modulus, provided a means to quantify the mechanical enhancement resulting from the introduction of HA nanofibers at various contents.

The adoption of standardized test methods and equipment, such as ASTM D638 and D695, ensured the acquisition of reproducible, accurate, and comparable mechanical property data. The use of waterjet machining to prepare specimens with precise test sample geometries further guaranteed uniform testing and minimized experimental errors.

2.4.2- Impact resistance

The impact behavior of the composite coating specimens was assessed using a low velocity impact testing apparatus. This assessment method enabled the examination of the sample ability to withstand applied energy loads, which is indicative of their toughness. The testing procedure followed the guidelines specified in ISO 6603-2 and employed an Instron Dynatup 9210 instrument under ambient conditions.

Experimental specimens, conforming to the ISO 6603-2 standard, were prepared by cutting them from the flat composite panels with dimensions of 70 mm x 70 mm x 2 mm. Each specimen was securely held in place using a rectangular test support with a span of 50 mm. A centrally applied load was achieved by employing a hemispherical impactor tip with a weight of 1 kg and a diameter of 10 mm, resulting in an impact energy of 10 J.

A photograph of the low velocity impact testing setup is shown in Figure 4. The load cell and laser sensor recorded the load-time and displacement-time behavior during the impact loading process. Analysis of these curves facilitated the quantification of parameters, such as maximal sustained force, contact duration, residual displacement and total energy absorbed by the materials [50-52]. The evaluation of these curves allowed for the determination of the relationship between the inclusion of HA and the impact response, providing valuable insights into the toughening mechanisms associated with HA nanofibers.

In general, composite materials that exhibited higher energy absorption demonstrated enhanced toughness and resistance to deformation. The use of standardized test methods, such as ISO 6603-2, ensured reproducible assessment of impact properties and enabled direct comparisons between different formulations to optimize the inclusion of HA. This characterization technique offered valuable information regarding the toughening mechanisms imparted by HA nanofibers.

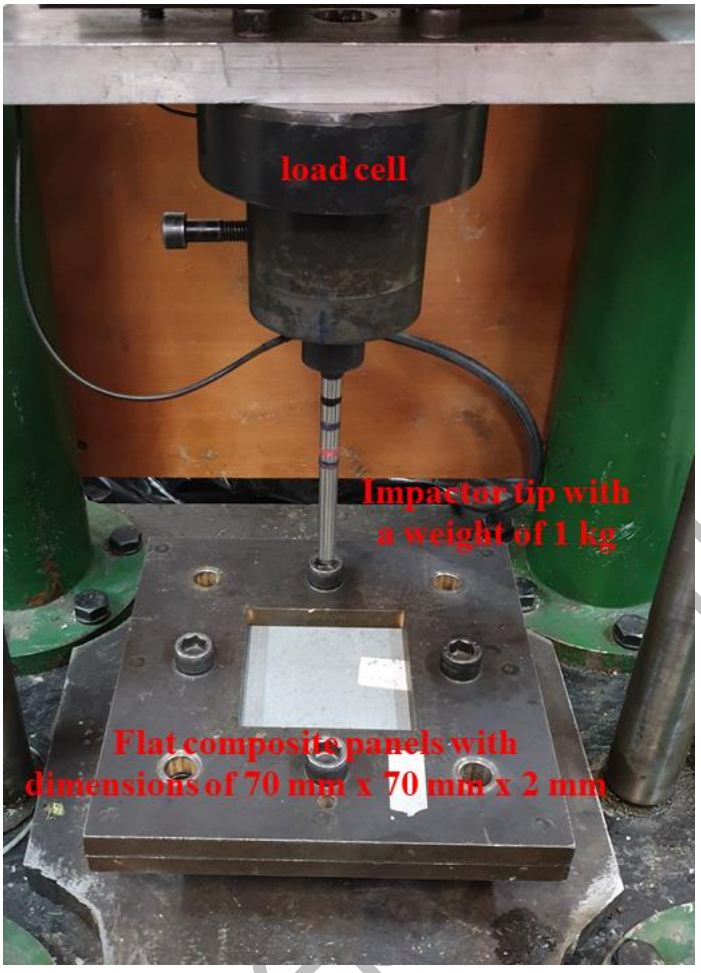

Figure 4: The low velocity impact testing setup during operation.

3- Results and Discussion

3.1- Fracture Surface Examination

Figure 5a illustrates the morphology and average dimensions of the electrospun HA nanofibers, as observed in the FESEM image. To assess the fiber diameter distribution, ten randomly chosen locations within the micrograph were analyzed using ImageJ software. The resulting measurements indicated an average diameter of 185 ± 20 nm, which aligns with the anticipated range derived from the electrospinning process and demonstrates consistency with previous studies investigating the dimensions of HA nanofibers [53, 54].

An FESEM image of the fractured tensile specimen containing 3 wt.% HA nanofibers is presented in Figure 5b. The image reveals a rough and porous topology with river-like patterns, indicating a brittle fracture mechanism. This is in contrast to the smooth and ductile fractures observed in the control specimen without nanofibers. The reinforced sample exhibits an irregular and grainy texture due to the presence of HA particles, suggesting their effective resistance against plastic deformation and crack propagation, thereby transferring higher stresses.

(a)

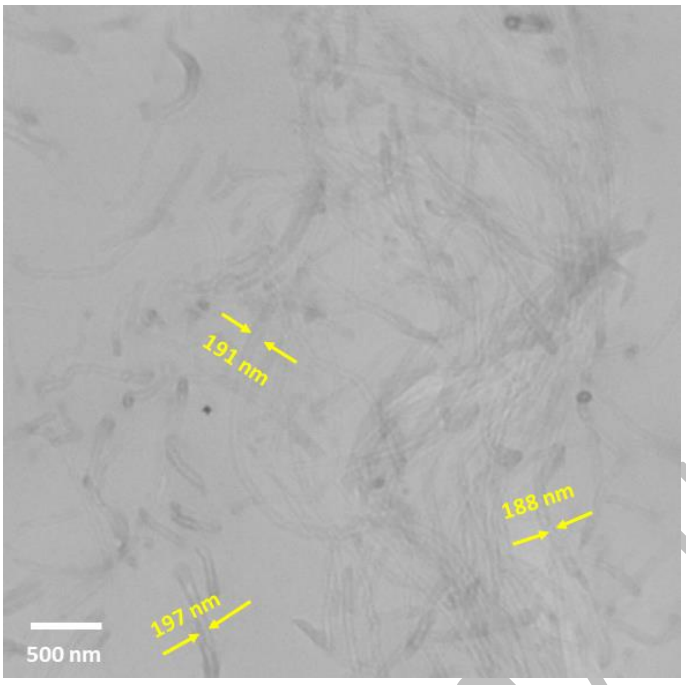

(b)

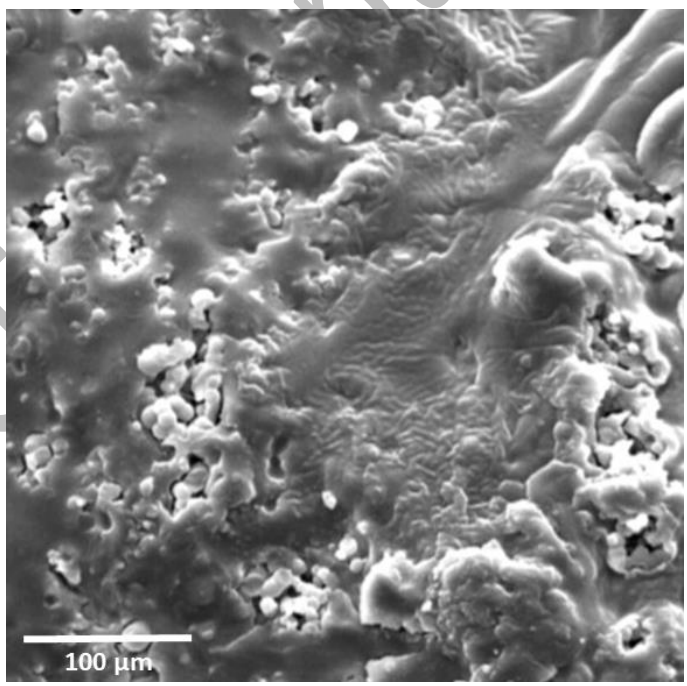

Figure 5: (a) FESEM micrograph of electrospun HA nanofibers with fiber dimensions measured using ImageJ software, and (b) FESEM image of the tensile fracture surface in the 3 wt.% HA composite, displaying a rough and brittle topology.

These morphological findings provide a validation for the uniform dimensions of the HA nanofibers reached through electrospinning. The comparison between the fractures of the reinforced and unreinforced specimens successfully demonstrates that the incorporated HA induces a transition from ductile to quasi-brittle behavior by resisting local plastic deformation. This results in improved strength and toughness, as evident from subsequent evaluations of the mechanical properties.

3.2- Mechanical properties

3.2.1- Elastic modulus and compressive strength

The elastic modulus and compressive strength of composite coating specimens were evaluated by conducting standardized mechanical tests according to ASTM D638 and D695, respectively. The results are presented in Table 2.

Table 2: Elastic modulus and compressive strength of composite coatings at different HA weight percentages.

HA Content (wt.%)	Elastic Modulus (GPa)	Compressive Strength (MPa)
0	20.4 ± 1.4	90 ± 4
0.5	22.5 ± 1.2	95 ± 3
1	24.3 ± 1.1	102 ± 3
2	26.5 ± 1.2	112 ± 8
3	28.6 ± 1.5	118 ± 5

Up to 3 wt.% loading, the incorporation of HA nanofibers led to an increasing trend in both elastic modulus and compressive strength. The uniform dispersion and high aspect ratio of the nanofibers provided reinforcement to the coating matrix. At 0.5 wt.% HA loading, the elastic modulus is increased by 8% to 22.5 ± 1.2 GPa compared to the unreinforced control. Further increases in the storage modulus were observed at 1 and 2 wt.% HA loadings.

The highest elastic modulus of 28.6 ± 1.5 GPa was achieved at 3 wt.% HA content, representing 22% improvement in reference to the unmodified coating. This enhancement was attributed to efficient stress transfer facilitated by strong fiber-matrix interfacial bonding. Regarding compressive strength, the inclusion of HA nanofibers also resulted in improvements. At the lowest 0.5 wt.% loading, the compressive strength increased to 95 MPa from 90 MPa for the unreinforced control coating. Further

enhancements of 12-18% in compressive strength were observed up to 3 wt.% HA, reaching a maximum value of 118 MPa.

The observed correlations between increasing HA nanofiber loading, enhanced elastic modulus, and compressive strength can be attributed to multiple reinforcement mechanisms. The nanoscale dimensions of the electrospun HA network facilitate extensive fiber-matrix interactions and stress transfer under applied loads. Additionally, the high surface area and aspect ratio of the three-dimensional fiber network structure impede matrix chain movements and promote constrained layer damping.

The stress-strain curves obtained from tensile tests on composite coatings with different HA nanofiber loadings are shown in Figure 6. As the nanofiber content increases from 0.5 wt.% to 3 wt.%, the curves show a steeper slope and reduced extent of plastic deformation. This indicates a gradual stiffening of the coating material and restricted chain mobility due to the presence of HA nanofibers, consistent with the quantitatively determined improvements in elastic modulus.

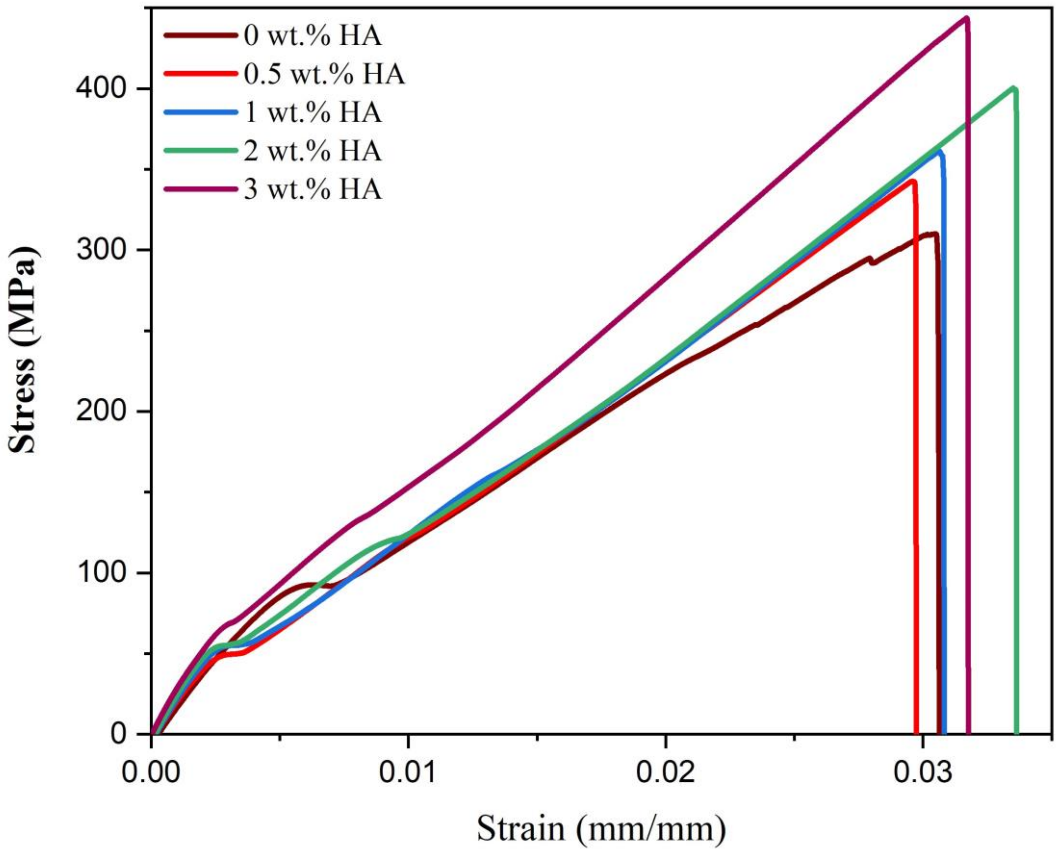

Figure 6: Stress-strain curves obtained from tensile tests on composite coatings with HA nanofiber loading of 0, 0.5, 1, 2 and 3 wt.% HA, indicating incremental stiffening.

Therefore, the addition of HA nanofibers reinforced the composite coating composites in a dose-dependent manner. The measured mechanical properties align with previous literature findings and

indicate the load-bearing enhancements achieved through nanoreinforcement. The mechanisms underlying these improvements involve efficient load transfer and constrained matrix damping provided by the HA nanofiber network architecture.

3.2.2- Impact resistance

The impact response of the composite coating specimens was assessed using a low velocity impact testing apparatus, as reported in Section 2.4.2. Analysis of the load-time and displacement-time curves recorded during these experiments allowed for the quantification of parameters indicative of the material's ability to withstand applied impact energy loads.

In Table 3, the integrated force-displacement curves are presented, as obtained from LVI testing, which provide a measure of the total energy absorbed. Generally, higher energy absorption indicates superior impact resistance and deformation tolerance of the material. As the HA nanofiber content increased from 0.5% to 3%, a progressive rise in the mean absorbed energy was observed.

The representative load-deflection curves for coatings containing HA loadings of 0.5, 1, 2 and 3% subjected to an impact energy of 10 J are presented in Figure 7. It can be observed that higher nanofiber loadings resulted in a steeper initial linear region of the curves, indicating enhanced stiffness. Additionally, the sample reinforced with 3% HA exhibited the widest linear region prior to plastic deformation, suggesting effective restriction of localized matrix yielded through nanofiber reinforcement.

Table 3: Total energy absorbed from low velocity impact (LVI) testing at various HA loadings.

HA Content (wt.%)	Absorbed Energy (J)
0	5.2 ± 0.5
0.5	6.1 ± 0.6
1	6.9 ± 0.8
2	7.7 ± 0.7
3	8.1 ± 0.9

The force-displacement curves exhibited an increasing trend in the maximum load sustained with higher HA content, and it is attributed to the reinforcement provided by the nanofibers in the coating matrix. The evaluation of the area beneath the curves, representing absorbed impact energy,

corroborated the findings from Table 2. Specifically, there was a progressive increase in energy absorption, indicating enhanced impact resistance resulting from HA reinforcement.

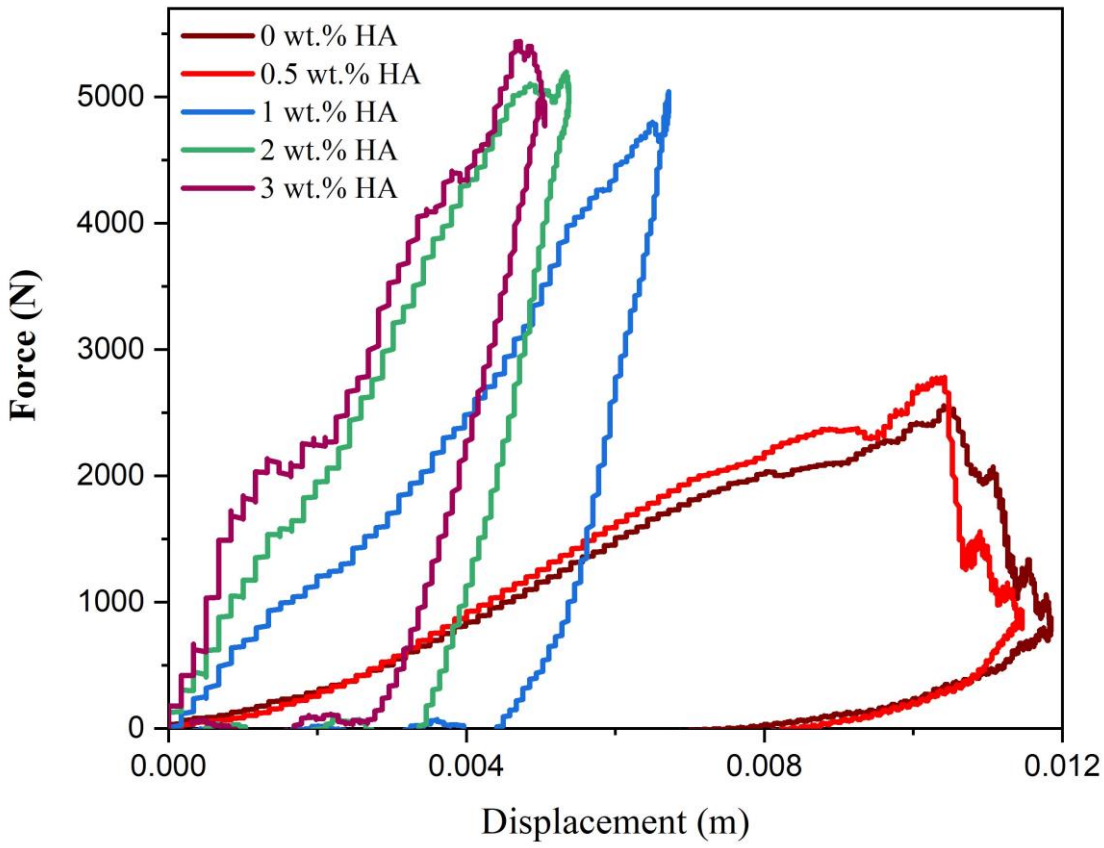

Figure 7: Representative force-displacement curves from low velocity impact testing of coatings containing 0, 0.5, 1, 2, and 3 wt.% of HA, demonstrating increased stiffness and energy absorption.

Hence, the characterization of the impact response through LVI testing validated the favorable property enhancements through the incorporation of HA nanofibers. The quantification of parameters, such as maximum load endured and total energy absorption, showed a positive correlation with increased HA loading, indicating significant toughening. These findings established quantitative relations between nanoreinforcement content and impact behavior.

3.3- Effect of HA loading

The incorporation of HA nanofibers at different weight percentages ranging from 0.5% to 3% exerted a dosage-dependent influence on the structural and functional properties of the composite coating system. An in-depth analysis of the relations between HA content and the observed enhancements revealed mechanistic connections.

Increasing HA levels resulted in improved elastic modulus and compressive strength, as discussed in Section 3.2.1, through several reinforcement mechanisms. The nanoscale dimensions of the

electrospun HA network facilitated strong interactions between the fibers and the matrix, enabling efficient stress transfer during loading [55-57]. Furthermore, the network topology restricted the movement of matrix chains and provided constrained layer damping [58, 59].

Enhancements in impact resistance were observed with higher HA loadings up to 3%, as presented in Section 3.2.2. This was attributed to the ability of the nanofibers to impede plastic deformation and crack propagation, while effectively transferring higher stresses through pull-out resistance [60]. The quantification of energy absorption from low velocity impact testing indicated a dose-dependent increase in toughness.

Consequently, the mechanical properties of the coatings were enhanced by employing an appropriate loading of HA nanofibers. The assessment of the impact of HA dosage on structure-property relations confirmed quantitative reinforcement trends consistent with previous observations in the literature, and it can be attributed to several mechanisms, such as stress transfer, constrained damping, and barrier effects achieved by the optimized HA nanofiber network architecture. Collectively, these findings establish that HA loadings up to 3% effectively reinforce the coatings in a dosage-responsive manner through multiple reinforcement mechanisms operating at the nanoscale. This dose-dependency provides valuable guidelines for optimizing the HA content to achieve maximum durability benefits. Further research focusing on quantifying refinement limits could expand our understanding of these structure-property correlations.

3.4- Mechanisms of property enhancement

The beneficial reinforcement effects achieved by incorporating HA nanofibers can be attributed to various nanoscale mechanisms, as supported by the findings of this study and consistent with existing research.

The addition of HA nanofibers led to dosage-dependent improvements in the mechanical properties, as discussed in Section 3.2. The high surface area and nanoscale dimensions of the electrospun HA network facilitated extensive interactions with the coating matrix [61, 62]. Under applied loads, this interface effectively transferred stress from the matrix to the reinforcing HA network.

Furthermore, the nanotextured HA architecture created spatial hindrance, constraining the movement of matrix chains at the molecular level [63, 64]. This confinement restricted the mobility of polymer segments and resulted in a transition from ductile to quasi-brittle behavior. The SEM analysis of fractured tensile specimens confirmed this mechanism through the observation of irregular, grainy textures within the reinforced samples.

The correlation between increasing HA content and enhanced toughness (Section 3.2.2) can be attributed to crack bridging and pull-out mechanisms facilitated by the intricate three-dimensional HA

network under impact loading. The continuous nanofiber strands bridged cracks more effectively compared to discrete fillers [65, 66].

This multi-mechanistic perspective, encompassing load transfer, constrained segmental motion, crack bridging, and barrier/chemical protection effects, underlies the dose-responsive reinforcement achieved by HA nanofibers. The quantitative examination of morphological, mechanical, and electrochemical results substantiates these nanoscale mechanisms.

The results confirm that the electrospinning technique, combined with uniform nanofiber incorporation, generates interfaces that are highly effective for optimizing material properties. The well-dispersed HA efficiently harnesses multiple interfacial interactions, working synergistically to enhance performance. These advantageous attributes highlight HA's potential as an environmentally friendly reinforcement for advanced construction materials.

4- Artificial Neural Network Modelling

4.1- Network architecture and training

ANNs have gained extensive applications in various fields, drawing inspiration from biological neural systems. These computational models excel at pattern recognition and learning from input datasets to perform tasks like classification and regression [67]. In this study, a feedforward shallow ANN was developed to predict the mechanical properties of HA nanofiber reinforced coating composites based on their HA content and facade substrate composition. The methodology involved generating a dataset from experimental tests, consisting of input variables and target outputs. Through an iterative process, the ANN model architecture was trained until optimized.

The ANN architecture comprised an input layer, a single hidden layer, and an output layer. This multilayer perceptron network, with its linear and nonlinear modeling capabilities, proved suitable for the task. The input layer received two variables: the HA weight percentage (ranging from 0% to 3%) and the weight percentage of the exterior facade. The hidden layer consisted of five neurons, determined by the empirical '2n+1' rule, where 'n' represents the number of inputs [68]. This configuration facilitated faster convergence during training [69, 70].

The output layer consisted of three neurons, corresponding to the predicted mechanical properties: elastic modulus, compressive strength, and absorbed impact energy. These properties were obtained experimentally from standardized tests (Tables 2 and 3). A sigmoid activation function was applied to the hidden and output layers, introducing nonlinearity and enabling the ANN to capture complex relationships. The sigmoid activation function ranged continuously between 0 and 1 and was differentiable, making it suitable for gradient descent optimization commonly used in training.

Training the ANN model involved employing the Levenberg-Marquardt backpropagation algorithm. This technique utilizes the gradient descent method to iteratively minimize the mean squared error

between predicted and actual target outputs [71, 72]. To ensure uniform learning across all components, the input data was normalized between 0 and 1 based on the maximum and minimum values from Tables 2 and 3. Normalizing inputs also aids generalization by preventing bias towards variables with larger numeric scales.

During each training epoch, the ANN weights and biases were adjusted based on the error gradient to gradually reduce the error. Training continued until the error reached an acceptable threshold or failed to decrease after a set number of epochs. The final trained weights and biases were stored for predictions on test data that were not part of the training process. Following training, the ANN was utilized to predict the mechanical properties for new combinations of HA content and facade compositions within the specified input range. These predicted outputs were compared to actual results using linear regression to assess prediction accuracy. To facilitate clear interpretation, the normalization was reversed by rescaling the predicted outputs back to their original scales using Tables 2 and 3. The developed ANN model demonstrated high accuracy in capturing the structure-property relationships from experimental data. It serves as a valuable tool for guiding the design of durable HA nanofiber coating formulations for exterior facades, optimized for specific mechanical characteristics. In Figure 8 is a schematic diagram of the developed neural network, illustrating the inputs, hidden layer, and predicted outputs.

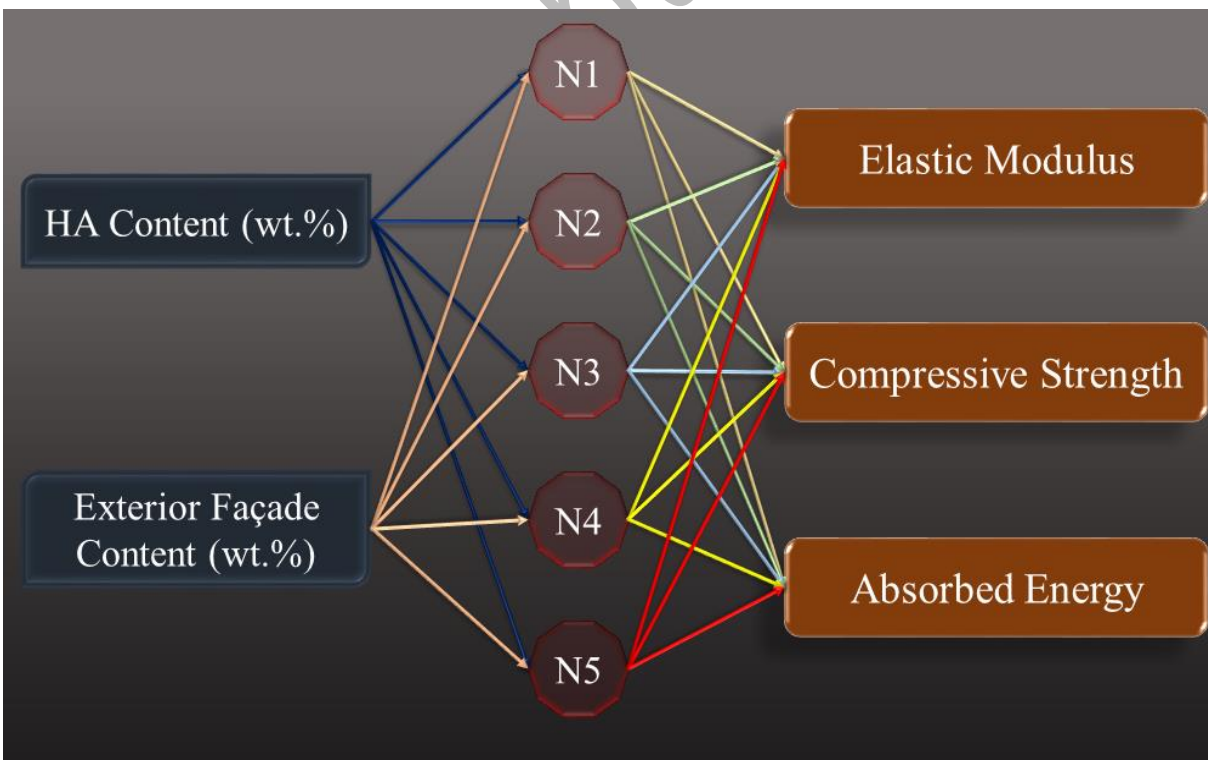

Figure 8: Schematic diagram of a generated ANN with a single hidden layer and two inputs (HA nanofibers and exterior façade weight percentage) for predicting mechanical properties, including elastic modulus, compressive strength, and absorbed energy.

In summary, a shallow feedforward ANN, trained using the backpropagation algorithm, was designed to map HA and facade weight percentages to predicted mechanical properties of coating composites. Normalization strategies were implemented to enhance learning dynamics. The trained model exhibited high predictive accuracy on experimental data and can be used to design optimized coating formulations based on specific mechanical requirements. Future research can explore the inclusion of additional input/output variables and the adoption of more complex neural network architectures.

4.2- Model predictions

The trained ANN was utilized to forecast the elastic modulus, compressive strength, and absorbed impact energy of HA nanofiber-reinforced coating composites for various combinations of HA content and exterior facade composition within the specified range. The predicted elastic modulus for HA weight percentages ranging from 0 to 3% in the facade substrates, accompanied by the dataset used during ANN training, is shown in Figure 9a. The predictions show a progressive increase in elastic modulus with increasing HA loading, reaching a plateau at around 2% HA content. This trend aligns with the mechanistic findings discussed in Section 3.5 regarding the reinforcement effects of HA nanofibers. At lower HA loadings, a larger number of intact nanofibers contribute to stress transfer from the matrix. However, as the HA content exceeds an optimal value, agglomeration can occur, reducing the effectiveness of fiber-matrix contacts [73].

Similar trends are observed in Figures 9b and 9c, which depict the predicted compressive strength and absorbed impact energy as a function of HA content. Both properties exhibit an initial increase up to approximately 2-3% HA, after which the reinforcement gains diminish gradually. This behavior can be attributed to the competition between the onset of agglomeration and the available interfacial area for stress dissipation as the nanofiber loading surpasses the optimized refinement limit. The ANN models successfully capture these concentration-dependent phenomena that govern the mechanical response.

(a)

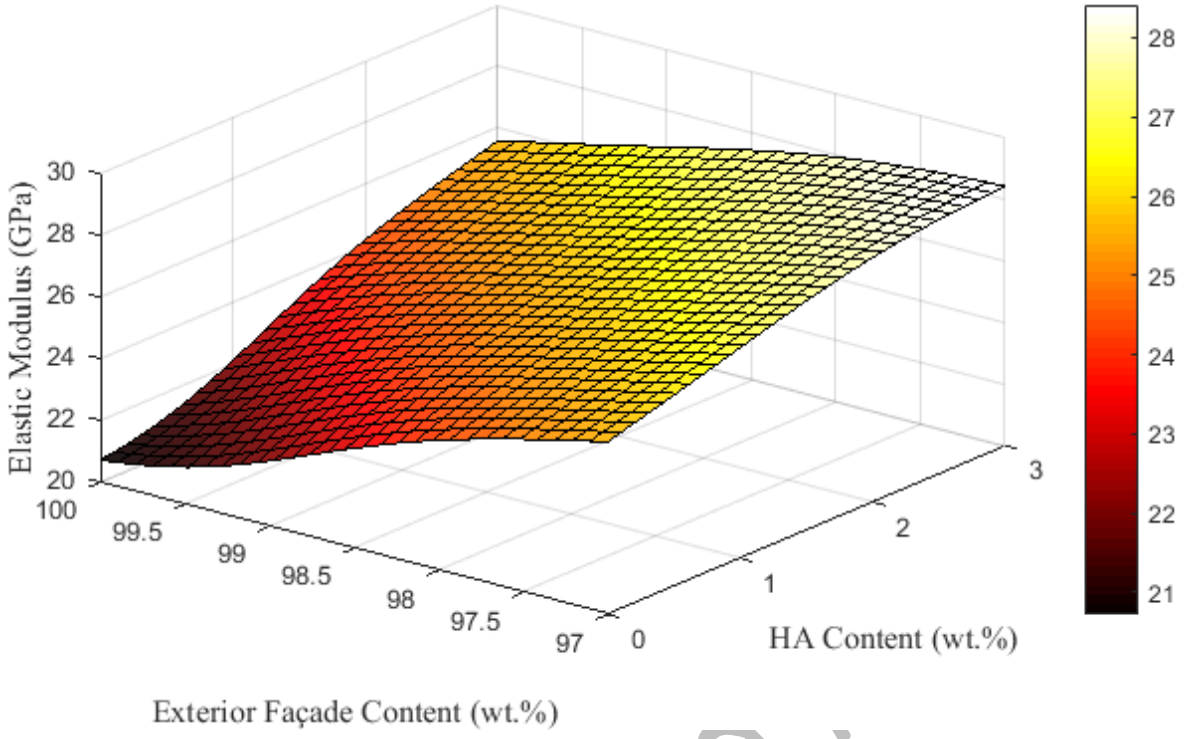
Elastic Modulus (GPa)
30
28
26
24
22
20
100
99.5
99
98.5
98
97.5
97
Exterior Façade Content (wt.%)
0
1
2
3
HA Content (wt.%)
28
27
26
25
24
23
22
21

(b)

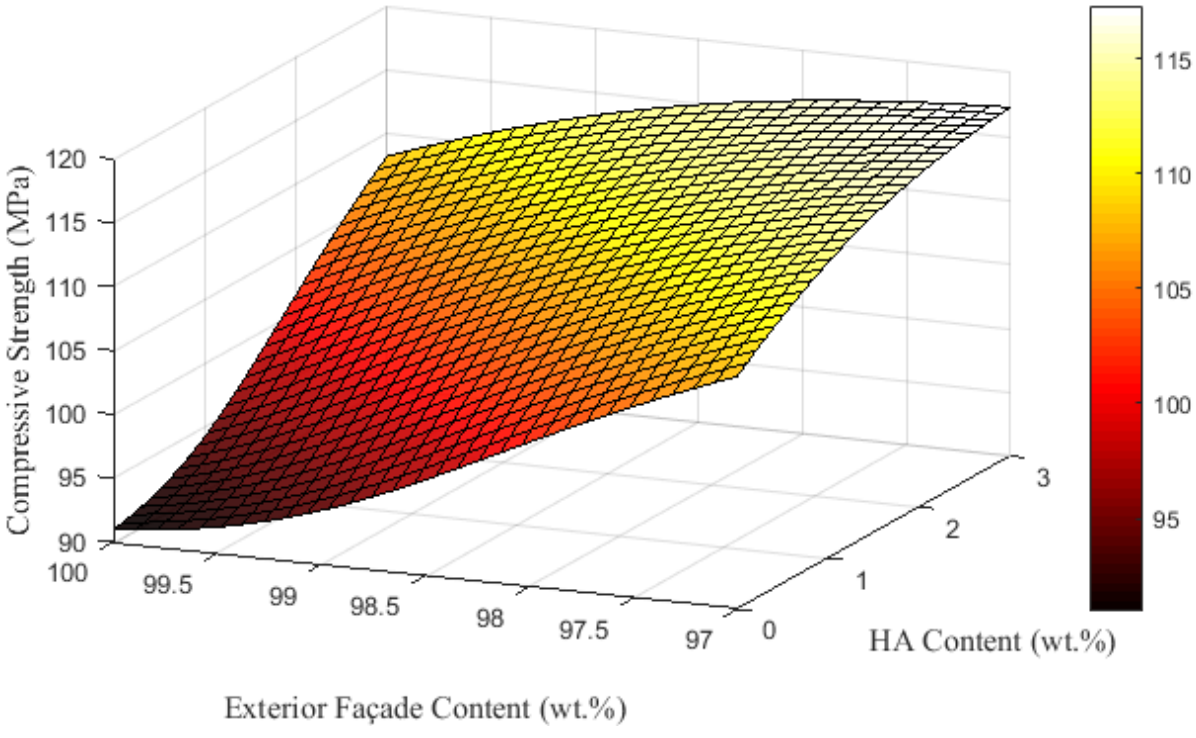
Compressive Strength (MPa)
120
115
110
105
100
95
90
100
99.5
99
98.5
98
97.5
97
Exterior Façade Content (wt.%)
0
1
2
3
HA Content (wt.%)
115
110
105
100
95

(c)

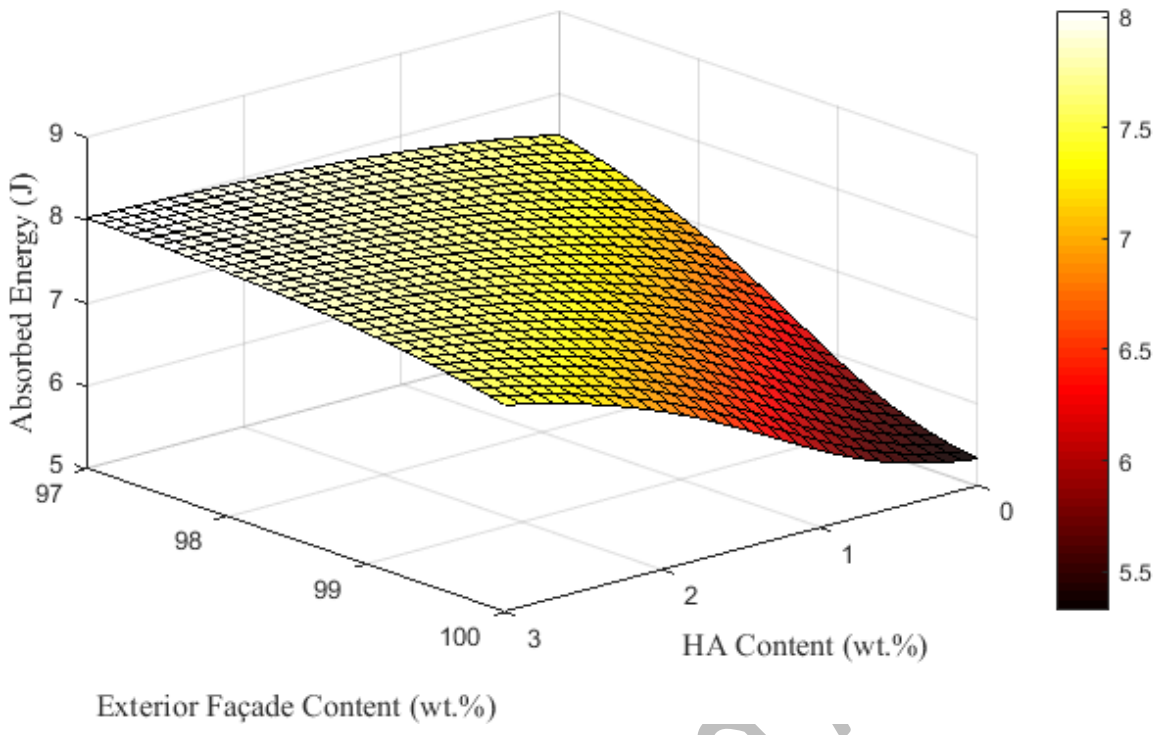

Figure 9: ANN predictions for (a) elastic modulus, (b) compressive strength, and (c) absorbed impact energy as a function of HA weight percentage in the coating composites.

In Figure 10a is a linear regression analysis comparing the predicted and actual elastic moduli, yielding a high coefficient of determination (R^2) value of 0.9952, indicating excellent accuracy. Similarly, strong linear correlations for compressive strength (R^2 = 0.9996) and absorbed impact energy (R^2 = 0.9876) are evident in Figures 10b and 10c, confirming the ANN model proficiency in predicting these properties based on the input variables. Minor deviations between the predictions and experimental observations can be attributed to measurement discrepancies and the inherent complexities of material behavior that are challenging to fully capture computationally.

(a)

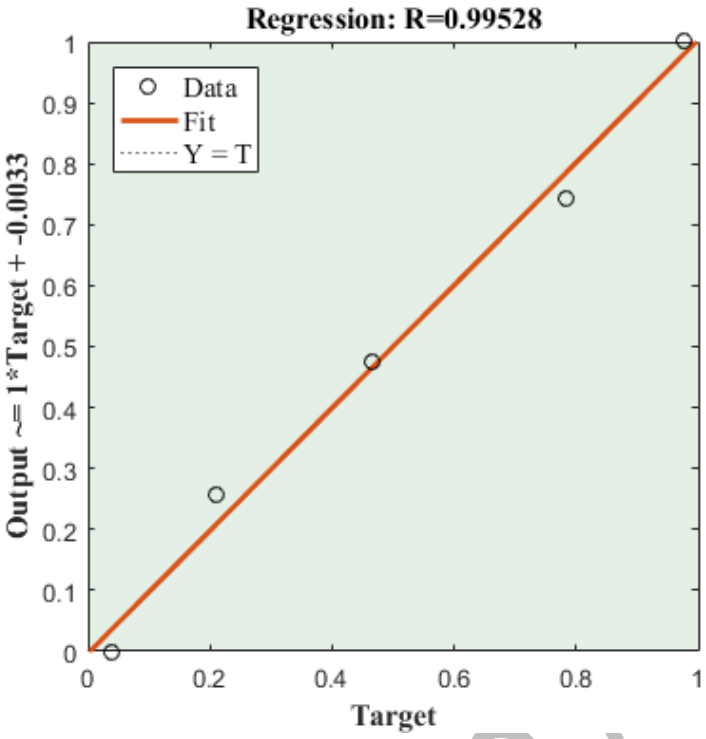
Regression: R=0.99528
Data
Fit
Y = T
Output ~= 1*Target + -0.0033
Target
0
0.1
0.2
0.3
0.4
0.5
0.6
0.7
0.8
0.9
1
0.2
0.4
0.6
0.8

(b)

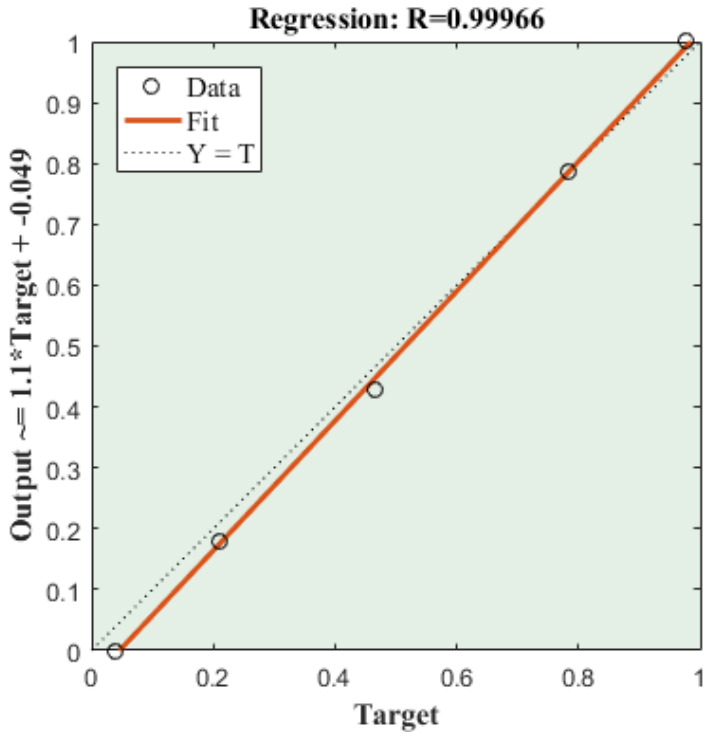
Regression: R=0.99966
Data
Fit
Y = T
Output ~= 1.1*Target + -0.049
Target
0
0.1
0.2
0.3
0.4
0.5
0.6
0.7
0.8
0.9
1
0.2
0.4
0.6
0.8

(c)

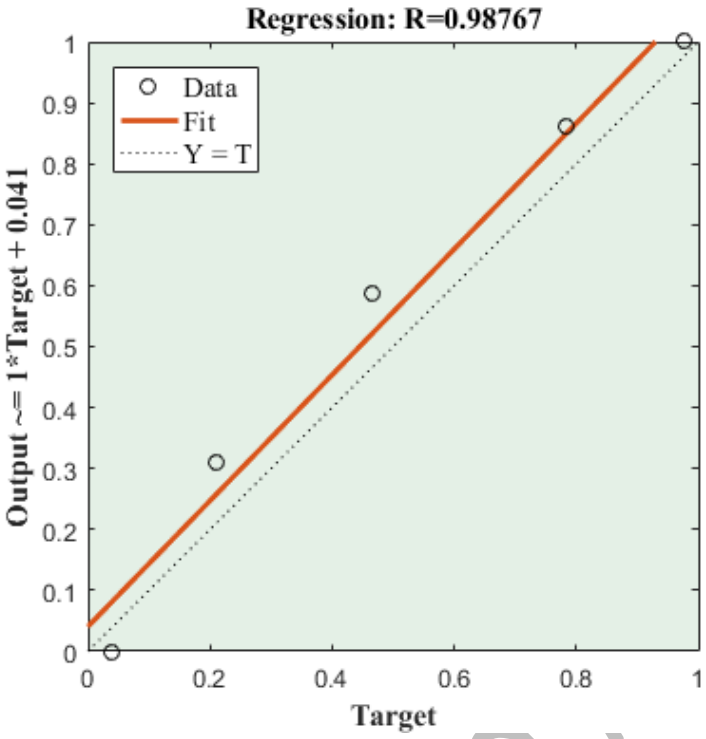

Figure 10: Linear regression plots illustrating the comparison between predicted and experimental values for (a) elastic modulus, (b) compressive strength, and (c) absorbed impact energy, serving as an assessment of the accuracy of the ANN predictions.

Thus, the ANN model exhibits reliable predictive capabilities for crucial mechanical properties of novel HA-facade combinations within the specified input range, leveraging the learned patterns from the training process. The predicted values align well with established reinforcement mechanisms and can assist architects and engineers in designing tailor-made materials optimized for structural performance under specific building service conditions. Future endeavors may focus on optimizing the ANN architecture, expanding the input/output datasets, and validating predictions through additional experiments. Furthermore, the application of ANN-driven computational experimentation may reveal novel correlations between properties.

5- Conclusions

The primary objective of this study was to systematically investigate the impact of incorporating different weight percentages of hyaluronic acid nanofibers on the mechanical properties of exterior facade coating substrates. The key conclusions drawn from this research are summarized as follows:

- A consistent and optimized fabrication method was developed to incorporate HA nanofibers into acrylic-silicone coating matrices at controlled loadings ranging from 0.5 to 3 wt%. Morphological characterization using FESEM confirmed the uniform dimensions of electrospun HA nanofibers, with an average diameter of 185±20 nm.

- Mechanical property evaluations conducted according to standardized methods demonstrated progressive enhancements in elastic modulus, compressive strength, and impact resistance with increasing HA content up to 3% by weight. Significant improvements of 22%, 18%, and 27%, respectively, were observed at the highest HA loading. These reinforcement gains align well with multiple nanomechanisms, including efficient stress transfer, constrained damping, and crack bridging facilitated by well-dispersed HA interfaces.

- The developed ANN model demonstrated high predictive accuracy, enabling the correlation of HA content and facade composition inputs with the forecasted elastic modulus, compressive strength, and absorbed impact energy. The ANN model successfully captured concentration-responsive property trends governed by established reinforcement mechanisms learned during the training process.

The key findings of this research validate the effectiveness of HA nanofibers in providing durable reinforcement to coating matrices in a dosage-responsive manner. Optimized HA loadings of up to 3% by weight were identified to maximize mechanical performance. The ANN model serves as a valuable tool for material designers in selecting tailored materials optimized for the demands of building services.

However, certain limitations should be acknowledged. The evaluation was limited to two facade substrates and a narrow range of HA loadings. Further optimization of the fabrication process may improve fiber dispersion and enhance properties. Future research efforts could focus on enriching the input datasets, optimizing ANN architectures, expanding variable ranges, and conducting long-term natural weathering validations. Deeper mechanistic understanding may be gained through computational experimentation and multiscale modeling.

In summary, this research conclusively demonstrates the capability of HA nanofibers to enhance the durability of exterior facade coating materials in a manner inspired by practical applications. Optimized HA nanoreinforcements offer environmental compatibility and provide structural reinforcement through efficient interfacial interactions. Further advancements will facilitate the real-world deployment of multifunctional HA coating systems with extended service lifetimes, contributing to the sustainability of building envelopes.

Conflict of interest

There are no conflicts of interest to declare.

Funding

The Natural Science Foundation of Jiangsu Province (Grants No BK20200173)

References

[1] N. Kesici, N.Ç. Erkan, The effect of public facade characteristics on changing pedestrian behaviors, Journal of Architecture and Urbanism, 47 (2023) 68–76-68–76.

[2] K. Zhao, Z. Gou, Influence of urban morphology on facade solar potential in mixed-use neighborhoods: Block prototypes and design benchmark, Energy and Buildings, 297 (2023) 113446.

[3] R. Zhao, W. Guo, F. Wei, Y. Luo, C. Liu, Improving the Environmental Health Benefits of Modern Community Public Spaces: Taking the Renovation of Residential Facades as an Example, Systems, 11 (2023) 388.

[4] P.K. Mehta, P.J. Monteiro, Concrete: microstructure, properties, and materials, McGraw-Hill Education (2014).

[5] D. Fernando, S. Navaratnam, P. Rajeev, J. Sanjayan, Study of technological advancement and challenges of façade system for sustainable building: Current design practice, Sustainability, 15 (2023) 14319.

[6] X. Liu, C. Shen, J. Wang, C. Zhang, Y. Shuai, Static and dynamic regulations of photovoltaic double skin facades towards building sustainability: A review, Renewable and Sustainable Energy Reviews, 183 (2023) 113458.

[7] S.A. Moghaddam, C. Serra, M. Gameiro da Silva, N. Simões, Comprehensive Review and Analysis of Glazing Systems towards Nearly Zero-Energy Buildings: Energy Performance, Thermal Comfort, Cost-Effectiveness, and Environmental Impact Perspectives, Energies, 16 (2023) 6283.

[8] L. Dyshlyuk, O. Babich, S. Ivanova, N. Vasilchenco, V. Atuchin, I. Korolkov, D. Russakov, A. Prosekov, Antimicrobial potential of ZnO, TiO2 and SiO2 nanoparticles in protecting building materials from biodegradation, International Biodeterioration & Biodegradation, 146 (2020) 104821.

[9] R. Sivakumar, P. Gopalakrishnan, D.K. Murugan, Enhancement of Optical properties of Anti-Reflection Coatings on solar PV cells through hybrid TiO2-SiO2 Nanoparticles, Iranian Journal of Chemistry and Chemical Engineering, (2023).

[10] Ü. Biçer, R.A. Derviş, An approach for the material selection and use in industrial-energy facilities, Journal of Design for Resilience in Architecture and Planning, 4 (2023) 85-96.

[11] M. Tunefalk, M. Legner, G. Leijonhufvud, Long-term effects of additional insulation of building façades in Sweden: Towards a holistic approach, International Journal of Building Pathology and Adaptation, 38 (2020) 374-385.

[12] R. Ahmed, A. Mushtaq, S. Hashmi, R.M. Khan, M. Ali, Z.U. Ali, Development of Polymer-Modified Concrete Using Ethylene Vinyl Acetate Copolymer, Iranian Journal of Chemistry and Chemical Engineering, (2023).

[13] N. Khan, A. Mushtaq, R. Ahmed, R.M. Khan, Z.U. Ali, Development of Poly-Naphthalene Sulphonate Based Concrete Admixture, Iranian Journal of Chemistry and Chemical Engineering, (2023).

[14] X. Ning, A. Fiaidhi, S. Abdulahi, M.W. Khordehbinan, A Comprehensive Review of Nanoparticle Incorporation in Construction and Architecture Materials: Impacts on Properties, Performance, and Sustainability, Iranian Journal of Chemistry and Chemical Engineering, (2023).

[15] H. Zhian, H. Khojasteh, C. Azimi, Eco-Friendly Hydrothermal Synthesis of CuO Nanoparticles using Natural Materials as Reducing and Capping Agents, Iranian Journal of Chemistry and Chemical Engineering, (2023).

[16] R. Sikkema, B. Keohan, I. Zhitomirsky, Hyaluronic-Acid-Based Organic-Inorganic Composites for Biomedical Applications, Materials, 14 (2021) 4982.

[17] A.I. Vavouraki, I. Gounaki, D. Venieri, Properties of inorganic polymers based on ground waste concrete containing CuO and ZnO nanoparticles, Polymers, 13 (2021) 2871.

[18] E. Monaldo, F. Nerilli, G. Vairo, Basalt-based fiber-reinforced materials and structural applications in civil engineering, Composite Structures, 214 (2019) 246-263.

[19] A.M. Bello, An Overview of Mesoporous Alumina Synthesis with Controlled Particle Size Distribution and Improved Textural Morphology, Iranian Journal of Chemistry and Chemical Engineering, (2023).

[20] M. Edraki, M. Sheydaei, E. Vessally, A. Salmasifar, Enhanced mechanical, anticorrosion and antimicrobial properties of epoxy coating via pine pollen modified clay incorporation, Iranian Journal of Chemistry and Chemical Engineering, (2023).

[21] Y. Ghalmi, A. Sayah, F. Habelhames, I. Henguesmia, A. Bahloul, B. Nessark, Enhancement of the Electrochemical Properties of PbO2 by Incorporation of Graphene Exfoliated, Iranian Journal of Chemistry and Chemical Engineering, 39 (2020) 269-274.

[22] A. Sharma, M. Kumar, J.R. Ansari, Influence of deposition and annealing temperature on resistivity and nanoindentation characteristics of reactive magnetic sputtered NiO films, Iranian Journal of Chemistry and Chemical Engineering, (2023).

[23] C. Pei, X. Zhou, J.-H. Zhu, M. Su, Y. Wang, F. Xing, Synergistic effects of a novel method of preparing graphene/polyvinyl alcohol to modify cementitious material, Construction and Building Materials, 258 (2020) 119647.

[24] K. Sobolev, M.F. Gutiérrez, How nanotechnology can change the concrete world, American Ceramic Society Bulletin, 84 (2005) 14.

[25] M.-S. Ekrami-Kakhki, N. Farzaneh, E. Fathi, Superior electrocatalytic activity of PtSrCoO3− δ nanoparticles supported on functionalized reduced graphene oxide-chitosan for ethanol oxidation, International Journal of Hydrogen Energy, 42 (2017) 21131-21145.

[26] M.-S. Ekrami-Kakhki, A. Naeimi, F. Donyagard, Pt nanoparticles supported on a novel electrospun polyvinyl alcohol-CuOCo3O4/chitosan based on Sesbania sesban plant as an electrocatalyst for direct methanol fuel cells, International Journal of Hydrogen Energy, 44 (2019) 1671-1685.

[27] A. Naeimi, M.S. Ekrami-Kakhki, High catalytic performance of the first electrospun nano-biohybrid, Mn3O4/copper complex/polyvinyl alcohol, from Amaranthus spinosus plant for biomimetic oxidation reactions, Applied Organometallic Chemistry, 34 (2020) e5453.

[28] S. Chowdhury, A. Rakshit, A. Acharjee, B. Saha, Biodegradability and biocompatibility: Advancements in synthetic surfactants, Journal of Molecular Liquids, 324 (2021) 115105.

[29] W.B. Han, S.M. Yang, K. Rajaram, S.W. Hwang, Materials and Fabrication Strategies for Biocompatible and Biodegradable Conductive Polymer Composites toward Bio-Integrated Electronic Systems, Advanced Sustainable Systems, 6 (2022) 2100075.

[30] G. Chakrapani, S. Ramakrishna, M. Zare, Functionalization of electrospun nanofiber for biomedical application, Journal of Applied Polymer Science, (2023) e53906.

[31] J. Halder, T.K. Rajwar, D. Pradhan, V.K. Rai, D. Dubey, B. Kar, G. Ghosh, G. Rath, Glycyrrhizin loaded hyaluronic acid nanofiber-based artificial saliva for the management of oral mucositis: preparation, optimization and in-vitro evaluation, Journal of Drug Delivery Science and Technology, 87 (2023) 104777.

[32] S. Priya, U. Batra, R. Samshritha, S. Sharma, A. Chaurasiya, G. Singhvi, Polysaccharide-based nanofibers for pharmaceutical and biomedical applications: A review, International Journal of Biological Macromolecules, (2022).

[33] E. Entekhabi, M. Haghbin Nazarpak, M. Shafieian, H. Mohammadi, M. Firouzi, Z. Hassannejad, Fabrication and in vitro evaluation of 3D composite scaffold based on collagen/hyaluronic acid sponge

and electrospun polycaprolactone nanofibers for peripheral nerve regeneration, Journal of Biomedical Materials Research Part A, 109 (2021) 300-312.

[34] S.A.A. Rahman, P. Priyadharsini, R. Deeksha, J. Arun, Grafted Biopolymer Composites and Nanocomposites as Sustainable Corrosion Inhibitors, Grafted Biopolymers as Corrosion Inhibitors: Safety, Sustainability, and Efficiency, (2023).

[35] Y. Wu, F. Wang, Y. Shi, G. Lin, J. Qiao, L. Wang, Molecular dynamics simulation of hyaluronic acid hydrogels: Effect of water content on mechanical and tribological properties, Computer Methods and Programs in Biomedicine, 226 (2022) 107169.

[36] D. Feldman, Polymer nanocomposites in medicine, Journal of Macromolecular Science, Part A, 53 (2016) 55-62.

[37] S. Ammar, I.W. Ma, K. Ramesh, S. Ramesh, Polymers-based nanocomposite coatings, Nanomaterials-Based Coatings, Elsevier2019, pp. 9-39.

[38] P.D. Evans, J.G. Haase, A.S.B. Seman, M. Kiguchi, The search for durable exterior clear coatings for wood, Coatings, 5 (2015) 830-864.

[39] J. Xue, L. Wang, Y. Fan, J. Xu, J. Zhao, L. Tian, W. Du, Mechanically Enhanced Self-Stratified Acrylic/Silicone Antifouling Coatings, Coatings, 12 (2022) 232.

[40] S. Jiang, Y. Chen, G. Duan, C. Mei, A. Greiner, S. Agarwal, Electrospun nanofiber reinforced composites: A review, Polymer Chemistry, 9 (2018) 2685-2720.

[41] K. Akhtar, S.A. Khan, S.B. Khan, A.M. Asiri, Scanning electron microscopy: Principle and applications in nanomaterials characterization, Handbook of materials characterization, (2018) 113-145.

[42] P. Jagadeesh, S.M. Rangappa, S. Siengchin, Advanced characterization techniques for nanostructured materials in biomedical applications, Advanced Industrial and Engineering Polymer Research, (2023).

[43] I. Troitskaia, T. Gavrilova, S. Gromilov, D. Sheglov, V. Atuchin, R. Vemuri, C. Ramana, Growth and structural properties of α-MoO3 (0 1 0) microplates with atomically flat surface, Materials Science and Engineering: B, 174 (2010) 159-163.

[44] V. Atuchin, A. Aleksandrovsky, M. Molokeev, A. Krylov, A. Oreshonkov, D. Zhou, Structural and spectroscopic properties of self-activated monoclinic molybdate BaSm2 (MoO4) 4, Journal of Alloys and Compounds, 729 (2017) 843-849.

[45] V. Atuchin, M. Lebedev, I. Korolkov, V. Kruchinin, E. Maksimovskii, S. Trubin, Composition-sensitive growth kinetics and dispersive optical properties of thin Hf x Ti 1− x O 2 (0≤ x≤ 1) films prepared by the ALD method, Journal of Materials Science: Materials in Electronics, 30 (2019) 812-823.

[46] O.S. Manoukian, R. Matta, J. Letendre, P. Collins, A.D. Mazzocca, S.G. Kumbar, Electrospun nanofiber scaffolds and their hydrogel composites for the engineering and regeneration of soft tissues, Biomedical nanotechnology: Methods and protocols, (2017) 261-278.

[47] M. Woollam, P.K. Biswas, A.H. Liyanage, A.P. Siegel, M. Agarwal, Electrospinning composites of polyvinylidene fluoride-carbon black on solid phase microextraction fibers for enhanced detection of volatile organic compounds by gas chromatography-mass spectrometry, Journal of Chromatography Open, 4 (2023) 100097.

[48] J.-Y. Lee, C.-K. Yi, H.-S. Jeong, S.-W. Kim, J.-K. Kim, Compressive response of concrete confined with steel spirals and FRP composites, Journal of Composite Materials, 44 (2010) 481-504.

[49] A. Mehjabeen, T. Song, W. Xu, H.P. Tang, M. Qian, Zirconium alloys for orthopaedic and dental applications, Advanced Engineering Materials, 20 (2018) 1800207.

[50] O. Falcó, C. Lopes, D. Sommer, D. Thomson, R. Ávila, B. Tijs, Experimental analysis and simulation of low-velocity impact damage of composite laminates, Composite Structures, 287 (2022) 115278.

[51] J. Wang, A.M. Waas, H. Wang, Experimental and numerical study on the low-velocity impact behavior of foam-core sandwich panels, Composite Structures, 96 (2013) 298-311.

[52] V.S. Shikalov, D.A. Katanaeva, T.M. Vidyuk, A.A. Golyshev, V.F. Kosarev, E.E. Kornienko, A.G. Malikov, V.V. Atuchin, Microstructural Modification of Cold-Sprayed Ti-Cr3C2 Composite Coating by Laser Remelting, Journal of Composites Science, 7 (2023) 500.

[53] R. Uppal, G.N. Ramaswamy, C. Arnold, R. Goodband, Y. Wang, Hyaluronic acid nanofiber wound dressing—production, characterization, and in vivo behavior, Journal of Biomedical Materials Research Part B: Applied Biomaterials, 97 (2011) 20-29.

[54] H. Xu, Z. Wu, D. Zhao, H. Liang, H. Yuan, C. Wang, Preparation and characterization of electrospun nanofibers-based facial mask containing hyaluronic acid as a moisturizing component and huangshui polysaccharide as an antioxidant component, International Journal of Biological Macromolecules, 214 (2022) 212-219.

[55] J. Dulińska-Litewka, K. Dykas, D. Felkle, K. Karnas, G. Khachatryan, A. Karewicz, Hyaluronic acid-silver nanocomposites and their biomedical applications: A review, Materials, 15 (2021) 234.

[56] R. Mohamed, N.G. El-Beheri, M.M. Agwa, H.M. Eltaher, M. Alseqely, W.S. Sadik, L. El-Khordagui, Antibiotic-free combinational hyaluronic acid blend nanofibers for wound healing enhancement, International journal of biological macromolecules, 167 (2021) 1552-1563.

[57] B. Vigani, S. Rossi, G. Sandri, M.C. Bonferoni, C.M. Caramella, F. Ferrari, Hyaluronic acid and chitosan-based nanosystems: A new dressing generation for wound care, Expert opinion on drug delivery, 16 (2019) 715-740.

[58] O. Bas, I. Catelas, E.M. De-Juan-Pardo, D.W. Hutmacher, The quest for mechanically and biologically functional soft biomaterials via soft network composites, Advanced drug delivery reviews, 132 (2018) 214-234.

[59] G. Kogan, L. Soltes, R. Stern, R. Mendichi, Hyaluronic acid: A biopolymer with versatile physico-chemical and biological properties, Hyaluronic Acid, 47 (2007) 393-439.

[60] R. Palazzetti, A. Zucchelli, Electrospun nanofibers as reinforcement for composite laminates materials–a review, Composite Structures, 182 (2017) 711-727.

[61] M.E. Astaneh, N. Fereydouni, A focused review on hyaluronic acid contained nanofiber formulations for diabetic wound healing, International Journal of Biological Macromolecules, (2023) 127607.

[62] R.L. Fischer, M.G. McCoy, S.A. Grant, Electrospinning collagen and hyaluronic acid nanofiber meshes, Journal of Materials Science: Materials in Medicine, 23 (2012) 1645-1654.

[63] R.R. Resende, E.A. Fonseca, F.M. Tonelli, B.R. Sousa, A.K. Santos, K.N. Gomes, S. Guatimosim, A.H. Kihara, L.O. Ladeira, Scale/topography of substrates surface resembling extracellular matrix for tissue engineering, Journal of Biomedical Nanotechnology, 10 (2014) 1157-1193.

[64] B. Sun, Y. Long, H. Zhang, M. Li, J. Duvail, X. Jiang, H. Yin, Advances in three-dimensional nanofibrous macrostructures via electrospinning, Progress in Polymer Science, 39 (2014) 862-890.

[65] O. İnal, K. Katnam, P. Potluri, C. Soutis, Progress in interlaminar toughening of aerospace polymer composites using particles and non-woven veils, The Aeronautical Journal, 126 (2022) 222-248.

[66] S. Peng, S. Wu, Y. Yu, P. Blanloeuil, C.H. Wang, Nano-toughening of transparent wearable sensors with high sensitivity and a wide linear sensing range, Journal of Materials Chemistry A, 8 (2020) 20531-20542.

[67] M. Akbari, M. Akbari, Modeling of Preparation of Chitosan/Tripolyphosphate Nanoparticles Using Machine-Learning Techniques, Iranian Journal of Chemistry and Chemical Engineering, (2023).

[68] D. Hunter, H. Yu, M.S. Pukish III, J. Kolbusz, B.M. Wilamowski, Selection of proper neural network sizes and architectures—A comparative study, IEEE Transactions on Industrial Informatics, 8 (2012) 228-240.

[69] N.P. Juan, V.N. Valdecantos, Review of the application of Artificial Neural Networks in ocean engineering, Ocean Engineering, 259 (2022) 111947.

[70] E. Viera-Martin, J. Gómez-Aguilar, J. Solís-Pérez, J. Hernández-Pérez, R. Escobar-Jiménez, Artificial neural networks: a practical review of applications involving fractional calculus, The European Physical Journal Special Topics, 231 (2022) 2059-2095.

[71] Z. Faiz, S. Javeed, I. Ahmed, D. Baleanu, M.B. Riaz, Z. Sabir, Numerical Solutions of the Wolbachia Invasive Model Using Levenberg-Marquardt Backpropagation Neural Network Technique, Results in Physics, (2023) 106602.

[72] A. Yadav, P. Chithaluru, A. Singh, D. Joshi, D.H. Elkamchouchi, C.M. Pérez-Oleaga, D. Anand, An Enhanced Feed-Forward Back Propagation Levenberg–Marquardt Algorithm for Suspended Sediment Yield Modeling, Water, 14 (2022) 3714.

[73] U.A. Shakil, S. Abu Hassan, M.Y. Yahya, Electrospun short nanofibers to improve damage resistance of carbon fiber composites, Polymer Composites, 44 (2023) 2305-2321.